

Measurements of the branching fractions for the semi-leptonic decays $D_s^+ \rightarrow \phi e^+ \nu_e, \phi \mu^+ \nu_\mu, \eta \mu^+ \nu_\mu$ and $\eta' \mu^+ \nu_\mu$

M. Ablikim¹, M. N. Achasov^{9,e}, S. Ahmed¹⁴, M. Albrecht⁴, A. Amoroso^{53A,53C}, F. F. An¹, Q. An^{50,a}, J. Z. Bai¹, Y. Bai³⁹, O. Bakina²⁴, R. Baldini Ferroli^{20A}, Y. Ban³², D. W. Bennett¹⁹, J. V. Bennett⁵, N. Berger²³, M. Bertani^{20A}, D. Bettoni^{21A}, J. M. Bian⁴⁷, F. Bianchi^{53A,53C}, E. Boger^{24,c}, I. Boyko²⁴, R. A. Briere⁵, H. Cai⁵⁵, X. Cai^{1,a}, O. Cakir^{43A}, A. Calcaterra^{20A}, G. F. Cao¹, S. A. Cetin^{43B}, J. Chai^{53C}, J. F. Chang^{1,a}, G. Chelkov^{24,c,d}, G. Chen¹, H. S. Chen¹, J. C. Chen¹, M. L. Chen^{1,a}, S. J. Chen³⁰, X. R. Chen²⁷, Y. B. Chen^{1,a}, X. K. Chu³², G. Cibinetto^{21A}, H. L. Dai^{1,a}, J. P. Dai^{35,j}, A. Dbeyssi¹⁴, D. Dedovich²⁴, Z. Y. Deng¹, A. Denig²³, I. Denysenko²⁴, M. Destefanis^{53A,53C}, F. De Mori^{53A,53C}, Y. Ding²⁸, C. Dong³¹, J. Dong^{1,a}, L. Y. Dong¹, M. Y. Dong^{1,a}, O. Dorjkhaidav²², Z. L. Dou³⁰, S. X. Du⁵⁷, P. F. Duan¹, J. Fang^{1,a}, S. S. Fang¹, X. Fang^{50,a}, Y. Fang¹, R. Farinelli^{21A,21B}, L. Fava^{53B,53C}, S. Fegan²³, F. Feldbauer²³, G. Felici^{20A}, C. Q. Feng^{50,a}, E. Fioravanti^{21A}, M. Fritsch^{14,23}, C. D. Fu¹, Q. Gao¹, X. L. Gao^{50,a}, Y. Gao⁴², Y. G. Gao⁶, Z. Gao^{50,a}, I. Garzia^{21A}, K. Goetzen¹⁰, L. Gong³¹, W. X. Gong^{1,a}, W. Gradl²³, M. Greco^{53A,53C}, M. H. Gu^{1,a}, S. Gu¹⁵, Y. T. Gu¹², A. Q. Guo¹, L. B. Guo²⁹, R. P. Guo¹, Y. P. Guo²³, Z. Haddadi²⁶, S. Han⁵⁵, X. Q. Hao¹⁵, F. A. Harris⁴⁵, K. L. He¹, X. Q. He⁴⁹, F. H. Heinsius⁴, T. Held⁴, Y. K. Heng^{1,a}, T. Holtmann⁴, Z. L. Hou¹, C. Hu²⁹, H. M. Hu¹, T. Hu^{1,a}, Y. Hu¹, G. S. Huang^{50,a}, J. S. Huang¹⁵, X. T. Huang³⁴, X. Z. Huang³⁰, Z. L. Huang²⁸, T. Hussain⁵², W. Ikegami Andersson⁵⁴, Q. Ji¹, Q. P. Ji¹⁵, X. B. Ji¹, X. L. Ji^{1,a}, X. S. Jiang^{1,a}, X. Y. Jiang³¹, J. B. Jiao³⁴, Z. Jiao¹⁷, D. P. Jin^{1,a}, S. Jin¹, Y. Jin⁴⁶, T. Johansson⁵⁴, A. Julin⁴⁷, N. Kalantar-Nayestanaki²⁶, X. L. Kang¹, X. S. Kang³¹, M. Kavatsyuk²⁶, B. C. Ke⁵, T. Khan^{50,a}, A. Khokkaz⁴⁸, P. Kiese²³, R. Kliemt¹⁰, L. Koch²⁵, O. B. Kolcu^{43B,h}, B. Kopf⁴, M. Kornicer⁴⁵, M. Kuemmel⁴, M. Kuhlmann⁴, A. Kupsc⁵⁴, W. Kühn²⁵, J. S. Lange²⁵, M. Lara¹⁹, P. Larin¹⁴, L. Lavezzi^{53C,1}, H. Leithoff²³, C. Leng^{53C}, C. Li⁵⁴, Cheng Li^{50,a}, D. M. Li⁵⁷, F. Li^{1,a}, F. Y. Li³², G. Li¹, H. B. Li¹, H. J. Li¹, J. C. Li¹, Jin Li³³, K. Li¹³, K. Li³⁴, K. J. Li⁴¹, Lei Li³, P. L. Li^{50,a}, P. R. Li^{7,44}, Q. Y. Li³⁴, T. Li³⁴, W. D. Li¹, W. G. Li¹, X. L. Li³⁴, X. N. Li^{1,a}, X. Q. Li³¹, Z. B. Li⁴¹, H. Liang^{50,a}, Y. F. Liang³⁷, Y. T. Liang²⁵, G. R. Liao¹¹, D. X. Lin¹⁴, B. Liu^{35,j}, B. J. Liu¹, C. X. Liu¹, D. Liu^{50,a}, F. H. Liu³⁶, Fang Liu¹, Feng Liu⁶, H. B. Liu¹², H. H. Liu¹⁶, H. H. Liu¹, H. M. Liu¹, J. B. Liu^{50,a}, J. P. Liu⁵⁵, J. Y. Liu¹, K. Liu⁴², K. Y. Liu²⁸, Ke Liu⁶, L. D. Liu³², P. L. Liu^{1,a}, Q. Liu⁴⁴, S. B. Liu^{50,a}, X. Liu²⁷, Y. B. Liu³¹, Z. A. Liu^{1,a}, Zhiqing Liu²³, Y. F. Long³², X. C. Lou^{1,a,g}, H. J. Lu¹⁷, J. G. Lu^{1,a}, Y. Lu¹, Y. P. Lu^{1,a}, C. L. Luo²⁹, M. X. Luo⁵⁶, X. L. Luo^{1,a}, X. R. Lyu⁴⁴, F. C. Ma²⁸, H. L. Ma¹, L. L. Ma³⁴, M. M. Ma¹, Q. M. Ma¹, T. Ma¹, X. N. Ma³¹, X. Y. Ma^{1,a}, Y. M. Ma³⁴, F. E. Maas¹⁴, M. Maggiora^{53A,53C}, A. S. Magnoni^{20B}, Q. A. Malik⁵², Y. J. Mao³², Z. P. Mao¹, S. Marcello^{53A,53C}, Z. X. Meng⁴⁶, J. G. Messchendorp²⁶, G. Mezzadri^{21B}, J. Min^{1,a}, T. J. Min¹, R. E. Mitchell¹⁹, X. H. Mo^{1,a}, Y. J. Mo⁶, C. Morales Morales¹⁴, G. Morello^{20A}, N. Yu. Muchnoi^{9,e}, H. Muramatsu⁴⁷, P. Musiol⁴, A. Mustafa⁴, Y. Nefedov²⁴, F. Nerling¹⁰, I. B. Nikolaev^{9,e}, Z. Ning^{1,a}, S. Nisar⁸, S. L. Niu^{1,a}, X. Y. Niu¹, S. L. Olsen³³, Q. Ouyang^{1,a}, S. Pacetti^{20B}, Y. Pan^{50,a}, M. Papenbrock⁵⁴, P. Patteri¹⁴, M. Pelizaeus⁴, J. Pellegrino^{53A,53C}, H. P. Peng^{50,a}, K. Peters^{10,i}, J. Pettersson⁵⁴, J. L. Ping²⁹, R. G. Ping¹, R. Poling⁴⁷, V. Prasad^{40,50}, H. R. Qi², M. Qi³⁰, S. Qian^{1,a}, C. F. Qiao⁴⁴, N. Qin⁵⁵, X. S. Qin¹, Z. H. Qin^{1,a}, J. F. Qiu¹, K. H. Rashid^{52,k}, C. F. Redmer²³, M. Richter⁴, M. Ripka²³, M. Rolo^{53C}, G. Rong¹, Ch. Rosner¹⁴, X. D. Ruan¹², A. Sarantsev^{24,f}, M. Savrie^{21B}, C. Schnier⁴, K. Schoenning⁵⁴, W. Shan³², M. Shao^{50,a}, C. P. Shen², P. X. Shen³¹, X. Y. Shen¹, H. Y. Sheng¹, J. J. Song³⁴, W. M. Song³⁴, X. Y. Song¹, S. Sosio^{53A,53C}, C. Sowa⁴, S. Spataro^{53A,53C}, G. X. Sun¹, J. F. Sun¹⁵, L. Sun⁵⁵, S. S. Sun¹, X. H. Sun¹, Y. J. Sun^{50,a}, Y. K. Sun^{50,a}, Y. Z. Sun¹, Z. J. Sun^{1,a}, Z. T. Sun¹⁹, C. J. Tang³⁷, G. Y. Tang¹, X. Tang¹, I. Tapan^{43C}, M. Tiemens²⁶, B. T. Tsednee²², I. Uman^{43D}, G. S. Varner⁴⁵, B. Wang¹, B. L. Wang⁴⁴, D. Wang³², D. Y. Wang³², Dan Wang⁴⁴, K. Wang^{1,a}, L. L. Wang¹, L. S. Wang¹, M. Wang³⁴, P. Wang¹, P. L. Wang¹, W. P. Wang^{50,a}, X. F. Wang⁴², Y. D. Wang¹⁴, Y. F. Wang^{1,a}, Y. Q. Wang²³, Z. Wang^{1,a}, Z. G. Wang^{1,a}, Z. H. Wang^{50,a}, Z. Y. Wang¹, Z. Y. Wang¹, T. Weber²³, D. H. Wei¹¹, J. H. Wei³¹, P. Weidenkaff²³, S. P. Wen¹, U. Wiedner⁴, M. Wolke⁵⁴, L. H. Wu¹, L. J. Wu¹, Z. Wu^{1,a}, L. Xia^{50,a}, Y. Xia¹⁸, D. Xiao¹, H. Xiao⁵¹, Y. J. Xiao¹, Z. J. Xiao²⁹, Y. G. Xie^{1,a}, Y. H. Xie⁶, X. A. Xiong¹, Q. L. Xiu^{1,a}, G. F. Xu¹, J. J. Xu¹, L. Xu¹, Q. J. Xu¹³, Q. N. Xu⁴⁴, X. P. Xu³⁸, L. Yan^{53A,53C}, W. B. Yan^{50,a}, W. C. Yan², Y. H. Yan¹⁸, H. J. Yang^{35,j}, H. X. Yang¹, L. Yang⁵⁵, Y. H. Yang³⁰, Y. X. Yang¹¹, M. Ye^{1,a}, M. H. Ye⁷, J. H. Yin¹, Z. Y. You⁴¹, B. X. Yu^{1,a}, C. X. Yu³¹, J. S. Yu²⁷, C. Z. Yuan¹, Y. Yuan¹, A. Yuncu^{43B,b}, A. A. Zafar⁵², Y. Zeng¹⁸, Z. Zeng^{50,a}, B. X. Zhang¹, B. Y. Zhang^{1,a}, C. C. Zhang¹, D. H. Zhang¹, H. H. Zhang⁴¹, H. Y. Zhang^{1,a}, J. Zhang¹, J. L. Zhang¹, J. Q. Zhang¹, J. W. Zhang^{1,a}, J. Y. Zhang¹, J. Z. Zhang¹, K. Zhang¹, L. Zhang⁴², S. Q. Zhang³¹, X. Y. Zhang³⁴, Y. Zhang¹, Y. Zhang¹, Y. H. Zhang^{1,a}, Y. T. Zhang^{50,a}, Yu Zhang⁴⁴, Z. H. Zhang⁶, Z. P. Zhang⁵⁰, Z. Y. Zhang⁵⁵, G. Zhao¹, J. W. Zhao^{1,a}, J. Y. Zhao¹, J. Z. Zhao^{1,a}, Lei Zhao^{50,a}, Ling Zhao¹, M. G. Zhao³¹, Q. Zhao¹, S. J. Zhao⁵⁷, T. C. Zhao¹, Y. B. Zhao^{1,a}, Z. G. Zhao^{50,a}, A. Zhemchugov^{24,c}, B. Zheng^{14,51}, J. P. Zheng^{1,a}, W. J. Zheng³⁴, Y. H. Zheng⁴⁴, B. Zhong²⁹, L. Zhou^{1,a}, X. Zhou⁵⁵, X. K. Zhou^{50,a}, X. R. Zhou^{50,a}, X. Y. Zhou¹, Y. X. Zhou^{12,a}, J. Zhu⁴¹, K. Zhu¹, K. J. Zhu^{1,a}, S. Zhu¹, S. H. Zhu⁴⁹, X. L. Zhu⁴², Y. C. Zhu^{50,a}, Y. S. Zhu¹, Z. A. Zhu¹, J. Zhuang^{1,a}, B. S. Zou¹, J. H. Zou¹

(BESIII Collaboration)

¹ Institute of High Energy Physics, Beijing 100049, People's Republic of China

² Beihang University, Beijing 100191, People's Republic of China

³ Beijing Institute of Petrochemical Technology, Beijing 102617, People's Republic of China

⁴ Bochum Ruhr-University, D-44780 Bochum, Germany

⁵ Carnegie Mellon University, Pittsburgh, Pennsylvania 15213, USA

⁶ Central China Normal University, Wuhan 430079, People's Republic of China

⁷ China Center of Advanced Science and Technology, Beijing 100190, People's Republic of China

⁸ COMSATS Institute of Information Technology, Lahore, Defence Road, Off Raiwind Road, 54000 Lahore, Pakistan

⁹ G.I. Budker Institute of Nuclear Physics SB RAS (BINP), Novosibirsk 630090, Russia

¹⁰ GSI Helmholtzcentre for Heavy Ion Research GmbH, D-64291 Darmstadt, Germany

¹¹ Guangxi Normal University, Guilin 541004, People's Republic of China

¹² Guangxi University, Nanning 530004, People's Republic of China

¹³ Hangzhou Normal University, Hangzhou 310036, People's Republic of China

¹⁴ Helmholtz Institute Mainz, Johann-Joachim-Becher-Weg 45, D-55099 Mainz, Germany

- ¹⁵ Henan Normal University, Xinxiang 453007, People's Republic of China
- ¹⁶ Henan University of Science and Technology, Luoyang 471003, People's Republic of China
- ¹⁷ Huangshan College, Huangshan 245000, People's Republic of China
- ¹⁸ Hunan University, Changsha 410082, People's Republic of China
- ¹⁹ Indiana University, Bloomington, Indiana 47405, USA
- ²⁰ (A)INFN Laboratori Nazionali di Frascati, I-00044, Frascati, Italy; (B)INFN and University of Perugia, I-06100, Perugia, Italy
- ²¹ (A)INFN Sezione di Ferrara, I-44122, Ferrara, Italy; (B)University of Ferrara, I-44122, Ferrara, Italy
- ²² Institute of Physics and Technology, Peace Ave. 54B, Ulaanbaatar 13330, Mongolia
- ²³ Johannes Gutenberg University of Mainz, Johann-Joachim-Becher-Weg 45, D-55099 Mainz, Germany
- ²⁴ Joint Institute for Nuclear Research, 141980 Dubna, Moscow region, Russia
- ²⁵ Justus-Liebig-Universitaet Giessen, II. Physikalisches Institut, Heinrich-Buff-Ring 16, D-35392 Giessen, Germany
- ²⁶ KVI-CART, University of Groningen, NL-9747 AA Groningen, The Netherlands
- ²⁷ Lanzhou University, Lanzhou 730000, People's Republic of China
- ²⁸ Liaoning University, Shenyang 110036, People's Republic of China
- ²⁹ Nanjing Normal University, Nanjing 210023, People's Republic of China
- ³⁰ Nanjing University, Nanjing 210093, People's Republic of China
- ³¹ Nankai University, Tianjin 300071, People's Republic of China
- ³² Peking University, Beijing 100871, People's Republic of China
- ³³ Seoul National University, Seoul, 151-747 Korea
- ³⁴ Shandong University, Jinan 250100, People's Republic of China
- ³⁵ Shanghai Jiao Tong University, Shanghai 200240, People's Republic of China
- ³⁶ Shanxi University, Taiyuan 030006, People's Republic of China
- ³⁷ Sichuan University, Chengdu 610064, People's Republic of China
- ³⁸ Soochow University, Suzhou 215006, People's Republic of China
- ³⁹ Southeast University, Nanjing 211100, People's Republic of China
- ⁴⁰ State Key Laboratory of Particle Detection and Electronics, Beijing 100049, Hefei 230026, People's Republic of China
- ⁴¹ Sun Yat-Sen University, Guangzhou 510275, People's Republic of China
- ⁴² Tsinghua University, Beijing 100084, People's Republic of China
- ⁴³ (A)Ankara University, 06100 Tandogan, Ankara, Turkey; (B)Istanbul Bilgi University, 34060 Eyup, Istanbul, Turkey; (C)Uludag University, 16059 Bursa, Turkey; (D)Near East University, Nicosia, North Cyprus, Mersin 10, Turkey
- ⁴⁴ University of Chinese Academy of Sciences, Beijing 100049, People's Republic of China
- ⁴⁵ University of Hawaii, Honolulu, Hawaii 96822, USA
- ⁴⁶ University of Jinan, Jinan 250022, People's Republic of China
- ⁴⁷ University of Minnesota, Minneapolis, Minnesota 55455, USA
- ⁴⁸ University of Muenster, Wilhelm-Klemm-Str. 9, 48149 Muenster, Germany
- ⁴⁹ University of Science and Technology Liaoning, Anshan 114051, People's Republic of China
- ⁵⁰ University of Science and Technology of China, Hefei 230026, People's Republic of China
- ⁵¹ University of South China, Hengyang 421001, People's Republic of China
- ⁵² University of the Punjab, Lahore-54590, Pakistan
- ⁵³ (A)University of Turin, I-10125, Turin, Italy; (B)University of Eastern Piedmont, I-15121, Alessandria, Italy; (C)INFN, I-10125, Turin, Italy
- ⁵⁴ Uppsala University, Box 516, SE-75120 Uppsala, Sweden
- ⁵⁵ Wuhan University, Wuhan 430072, People's Republic of China
- ⁵⁶ Zhejiang University, Hangzhou 310027, People's Republic of China
- ⁵⁷ Zhengzhou University, Zhengzhou 450001, People's Republic of China
- ^a Also at State Key Laboratory of Particle Detection and Electronics, Beijing 100049, Hefei 230026, People's Republic of China
- ^b Also at Bogazici University, 34342 Istanbul, Turkey
- ^c Also at the Moscow Institute of Physics and Technology, Moscow 141700, Russia
- ^d Also at the Functional Electronics Laboratory, Tomsk State University, Tomsk, 634050, Russia
- ^e Also at the Novosibirsk State University, Novosibirsk, 630090, Russia
- ^f Also at the NRC "Kurchatov Institute", PNPI, 188300, Gatchina, Russia
- ^g Also at University of Texas at Dallas, Richardson, Texas 75083, USA
- ^h Also at Istanbul Arel University, 34295 Istanbul, Turkey
- ⁱ Also at Goethe University Frankfurt, 60323 Frankfurt am Main, Germany
- ^j Also at Key Laboratory for Particle Physics, Astrophysics and Cosmology, Ministry of Education; Shanghai Key Laboratory for Particle Physics and Cosmology; Institute of Nuclear and Particle Physics, Shanghai 200240, People's Republic of China
- ^k Government College Women University, Sialkot - 51310. Punjab, Pakistan.

By analyzing 482 pb^{-1} of e^+e^- collision data collected at the center-of-mass energy $\sqrt{s} = 4.009 \text{ GeV}$ with the BESIII detector, we measure the branching fractions for the semi-leptonic decays $D_s^+ \rightarrow \phi e^+ \nu_e$, $\phi \mu^+ \nu_\mu$, $\eta \mu^+ \nu_\mu$ and $\eta' \mu^+ \nu_\mu$ to be $\mathcal{B}(D_s^+ \rightarrow \phi e^+ \nu_e) = (2.26 \pm 0.45 \pm 0.09)\%$, $\mathcal{B}(D_s^+ \rightarrow \phi \mu^+ \nu_\mu) = (1.94 \pm 0.53 \pm 0.09)\%$, $\mathcal{B}(D_s^+ \rightarrow \eta \mu^+ \nu_\mu) = (2.42 \pm 0.46 \pm 0.11)\%$ and $\mathcal{B}(D_s^+ \rightarrow \eta' \mu^+ \nu_\mu) = (1.06 \pm 0.54 \pm 0.07)\%$, where the first and second uncertainties are statistical and systematic, respectively. The branching fractions for the three semi-muonic decays $D_s^+ \rightarrow \phi \mu^+ \nu_\mu$, $\eta \mu^+ \nu_\mu$ and $\eta' \mu^+ \nu_\mu$ are determined for the first time and that of

$D_s^+ \rightarrow \phi e^+ \nu_e$ is consistent with the world average value within uncertainties.

PACS numbers: 13.20.Fc, 12.38.Qk, 14.40.Lb

I. INTRODUCTION

The semi-leptonic (SL) decays of charmed mesons ($D^{0(+)}$ and D_s^+) provide an ideal window to explore heavy quark decays, as the strong and weak effects can be well separated in theory. The Operator Product Expansion (OPE) model predicts that the partial widths of the inclusive SL decays of $D^{0(+)}$ and D_s^+ mesons should be equal, up to non-factorizable components [1]. However, the CLEO collaboration reported a deviation 18% for inclusive partial widths between $D^{0(+)}$ and D_s^+ SL decays, which is more than 3 times of the experimental uncertainties [2]. Ref. [3] argues that this deviation may be due to that the spectator quark masses m_u and m_s differ on the scale of the daughter quark mass m_s in the Cabibbo-favored SL transition. Therefore, comprehensive or improved measurements of the branching fractions (BFs) for the exclusive SL decays of $D^{0(+)}$ and D_s^+ will benefit the understanding of this difference. Also, these measurements can serve to verify the theoretical calculations on these decay rates.

In recent years, the $D^{0(+)}$ SL decays have been well studied with good precision [4]. However, the progress in the studies of the D_s^+ SL decays is still relatively slow. Up to now, only D_s^+ semi-electronic decays have been investigated by various experiments [5–8] and no measurements of D_s^+ semi-muonic decays have been reported. We here report the first measurements of the BFs of the semi-muonic decays $D_s^+ \rightarrow \eta \mu^+ \nu_\mu$, $\eta' \mu^+ \nu_\mu$ and $\phi \mu^+ \nu_\mu$ as well as a measurement of the BF of the semi-electronic decay $D_s^+ \rightarrow \phi e^+ \nu_e$. Charge-conjugate decays are implied throughout this paper, unless otherwise stated. Among them, the studies of $D_s^+ \rightarrow \eta^{(\prime)} \mu^+ \nu_\mu$ may also shed light on $\eta - \eta'$ -glueball mixing [9], as their decay rates are expected to be sensitive to the $\eta - \eta'$ mixing angle [10].

In this paper, all measurements are preformed by analyzing the same data set as used in our previous measurements of $D_s^+ \rightarrow \eta^{(\prime)} e^+ \nu_e$ [8]. This data set, corresponding to an integrated luminosity of 482 pb^{-1} [11], was collected at the center-of-mass energy $\sqrt{s} = 4.009 \text{ GeV}$ with the BESIII detector.

II. BESIII AND MONTE CARLO

BESIII is a cylindrical spectrometer that is composed of a Helium-gas based main drift chamber (MDC), a plastic scintillator time-of-flight (TOF) system, a CsI (TI) electromagnetic calorimeter (EMC), a superconducting solenoid providing a 1.0 T magnetic field and a muon counter in the iron flux return yoke of the magnet. The momentum resolution of charged tracks in the MDC is 0.5% at a transverse momentum of 1 GeV/c, and the photon energy resolution is 2.5%(5.0%) at an energy of 1 GeV in the barrel (endcap) of the EMC. More details about BESIII detector are described in Ref. [12].

A GEANT4-based [13] Monte Carlo (MC) simulation software, which includes the geometric description of the BESIII detector and its response, is used to determine detection efficiencies and estimate background contributions. The simulation is implemented by the MC event generator KKMC [14] using EvtGen [15, 16], including the beam energy spread and the effects of initial-state radiation (ISR) [17]. Final-state radiation (FSR) of the charged tracks is simulated with the PHOTOS package [18]. An inclusive MC sample corresponding to an integrated luminosity of 11 fb^{-1} is generated at $\sqrt{s} = 4.009 \text{ GeV}$, which includes open charm production, ISR production of low-mass vector charmonium states, continuum light quark production, $\psi(4040)$ decays and QED events. The open charm processes are simulated with cross sections taken from Ref. [19]. The known decay modes of the charmonium states are produced by EvtGen with the BFs quoted from the Particle Data Group (PDG) [4], and the unknown decay modes are simulated by the LundCharm generator [20]. The SL decays of interest are simulated incorporating with the ISGW2 form-factor model [3].

III. DATA ANALYSIS

In e^+e^- collisions at $\sqrt{s} = 4.009 \text{ GeV}$, D_s^+ and D_s^- mesons can only be produced jointly without additional hadrons. Thus in an event where a D_s^- meson (called single-tag (ST) D_s^- meson) is fully reconstructed, the presence of a D_s^+ meson is guaranteed. In the systems recoiling against the ST D_s^- mesons, we can select the SL decays of interest (called double-tag (DT) events). For a specific ST mode i , the observed yields of ST (N_{ST}^i) and DT (N_{DT}^i) are given by

$$N_{\text{ST}}^i = 2N_{D_s^+ D_s^-} \mathcal{B}_{\text{ST}}^i \epsilon_{\text{ST}}^i \quad (1)$$

and

$$N_{\text{DT}}^i = 2N_{D_s^+ D_s^-} \mathcal{B}_{\text{ST}}^i \mathcal{B}_{\text{SL}}^i \epsilon_{\text{DT}}^i, \quad (2)$$

respectively. Where $N_{D_s^+ D_s^-}$ is the total number of $D_s^+ D_s^-$ pairs produced in data, $\mathcal{B}_{\text{ST}}^i$ and \mathcal{B}_{SL} are the BFs for the ST mode i and the SL decay of interest, ϵ_{ST}^i is the efficiency of reconstructing the ST mode i (called the ST efficiency), and ϵ_{DT}^i is the efficiency of simultaneously finding the ST mode i and the SL decay (called the DT efficiency). The efficiency of ST and DT are determined by MC simulation. In this analysis, the ST D_s^- mesons are reconstructed in ten hadronic decay modes: $K^+ K^- \pi^-$, $\phi \rho^-$, $K_S^0 K^+ \pi^- \pi^-$, $K_S^0 K^- \pi^+ \pi^- \pi^-$, $\eta \pi^-$, $\eta'_{\pi^+ \pi^-} \pi^-$, $\eta'_{\gamma \rho^0} \pi^-$ and $\eta \rho^-$. Candidates of K_S^0 , π^0 , η , ϕ , ρ^- , $\eta'_{\pi^+ \pi^-}$ and $\eta'_{\gamma \rho^0}$ are selected using $K_S^0 \rightarrow \pi^+ \pi^-$, $\pi^0 \rightarrow \gamma \gamma$, $\eta \rightarrow \gamma \gamma$, $\phi \rightarrow K^+ K^-$, $\rho^- \rightarrow \pi^0 \pi^-$, $\eta' \rightarrow \pi^+ \pi^- \eta$ and $\eta' \rightarrow \gamma \rho^0$ decays, respectively. The ST modes are selected separately

according to their charges. Based on Eq. (1) and Eq. (2), the BF of the SL decay can be determined according to

$$\mathcal{B}_{\text{SL}} = \frac{N_{\text{DT}}^{\text{tot}}}{N_{\text{ST}}^{\text{tot}} \bar{\epsilon}_{\text{SL}}}, \quad (3)$$

by considering the multiple ST modes, where $N_{\text{DT}}^{\text{tot}}$ and $N_{\text{ST}}^{\text{tot}}$ are the total yields of ST and DT events for multiple ST modes, $\bar{\epsilon}_{\text{SL}} = \sum_i (N_{\text{ST}}^i \epsilon_{\text{DT}}^i / \epsilon_{\text{ST}}^i) / N_{\text{ST}}^{\text{tot}}$ is the weighted efficiency of detecting the SL decay for the multi-ST mode according to the yields of different ST modes.

All charged tracks are required to be within a polar-angle (θ) range of $|\cos \theta| < 0.93$. The good charged tracks, except for those from K_S^0 decays, are required to originate within an interaction region defined by $V_{xy} < 1.0$ cm and $|V_z| < 10.0$ cm, where V_{xy} and $|V_z|$ are the distances of closest approach of the reconstructed track to the interaction point (IP) perpendicular to the beam direction and along the beam direction, respectively. Particle identification (PID) is implemented with the ionization energy loss (dE/dx) measured by the MDC and the time of flight recorded by the TOF. For each charged track, the combined confidence levels for pion and kaon hypotheses (CL_π and CL_K) are calculated, respectively. A pion (kaon) is identified by requiring $CL_\pi > 0$ and $CL_\pi > CL_K$ ($CL_K > 0$ and $CL_K > CL_\pi$). The K_S^0 candidates are reconstructed with two opposite charged tracks which satisfy $|V_z| < 20$ cm and are assumed to be pions without PID. A vertex constrained fit is performed to the $\pi^+\pi^-$ combinations, and the fitted track parameters are used in the further analysis. The distance L of the secondary vertex to the IP is also required to be positive with respect to the K_S^0 flight direction. K_S^0 candidates are required to have $\pi^+\pi^-$ invariant mass within (0.485, 0.511) GeV/ c^2 . Photon candidates are chosen from isolated clusters in the EMC. The deposited energy of a neutral cluster is required to be larger than 25 MeV in the barrel region ($|\cos \theta| < 0.80$) or 50 MeV in the end-cap region ($0.86 < |\cos \theta| < 0.92$). The angle between the photon candidate and the nearest charged track should be larger than 10° . To suppress electronic noise and energy deposits unrelated to the events, the difference between the EMC time and the event start time is required to be within (0, 700) ns. The π^0 and η candidates are reconstructed with $\gamma\gamma$ pair with invariant mass within (0.115, 0.150) and (0.510, 0.570) GeV/ c^2 . To improve momentum resolution, a kinematic fit is performed to constrain the $\gamma\gamma$ invariant mass to the nominal π^0 or η mass, and the fitted momenta of π^0 or η are used in the further analysis. To select candidates of ϕ , ρ^- , $\eta'_{\pi^+\pi^-\eta}$ and $\eta'_{\gamma\rho^0}$ mesons, the invariant masses of K^+K^- , $\pi^-\pi^0$, $\pi^+\pi^-\eta$ and $\gamma\rho^0$ are required to be within (1.005, 1.040), (0.570, 0.970), (0.943, 0.973) and (0.932, 0.980) GeV/ c^2 , respectively. For $\eta'_{\gamma\rho^0}$ candidate, the $\pi^+\pi^-$ invariant mass is additionally required to fall in (0.570, 0.970) GeV/ c^2 to reduce combinatorial backgrounds.

The ST D_s^- meson is identified using the energy difference $\Delta E \equiv E_{D_s^-} - E_{\text{beam}}$ and the beam-constrained mass $M_{\text{BC}} \equiv \sqrt{E_{\text{beam}}^2 - |\vec{p}_{D_s^-}|^2}$, where E_{beam} is the beam energy, $E_{D_s^-}$ and $|\vec{p}_{D_s^-}|$ are the total energy and momentum of the

ST D_s^- candidate in the e^+e^- center-of-mass frame. For each ST mode, only the one with the minimum $|\Delta E|$ is retained if there are multiple combinations in an event. To suppress combinatorial backgrounds, modes dependent ΔE requirements, which correspond to $(-3.0, +3.0)$ times of the resolution around the fitted ΔE peak, are imposed on the ST D_s^- candidates. Figure 1 shows the M_{BC} distributions of D_s^- candidates for individual ST mode. To obtain the ST yield (N_{ST}^i), we perform a maximum likelihood fit on these M_{BC} distributions. In the fits, we use the MC-simulated signal shape convoluted with a Gaussian function to model the D_s^- signals and an ARGUS function [21] to describe the combinatorial backgrounds. The events with M_{BC} within a mass window of $(-4.0, +5.0)$ times of the resolution around the D_s^- nominal mass [4] (called M_{BC} signal region) are kept for further analysis. For each ST mode, the ST yield is obtained by integrating the D_s^- signal over the corresponding M_{BC} signal region. The ST efficiency for the individual mode (ϵ_{ST}^i) is determined by analyzing the inclusive MC sample. Table I summarizes the requirements on ΔE and M_{BC} , the ST yields in data and the ST efficiencies. The total ST yield ($N_{\text{ST}}^{\text{tot}}$) is 13092 ± 247 .

The SL decays $D_s^+ \rightarrow \phi e^+ \nu_e$, $\phi \mu^+ \nu_\mu$, $\eta \mu^+ \nu_\mu$ and $\eta' \mu^+ \nu_\mu$ are selected recoiling against the ST D_s^- mesons. The charge of the electron (muon) candidate is required to be opposite to that of the ST D_s^- meson. For electron (muon) PID, the dE/dx , TOF and EMC information is used to form the combined confidence levels for electron, muon, pion and kaon hypotheses (CL_e , CL_μ , CL_π and CL_K). The electron candidates should satisfy $CL_e / (CL_e + CL_\pi + CL_K) > 0.8$ and $CL_e > 0.001$, while the muon candidates are required $CL_\mu > CL_e$, $CL_\mu > CL_K$ and $CL_\mu > 0.001$. It is required that there is no extra charged track except for those used in the DT event selection. For $D_s^+ \rightarrow \eta^{(\prime)} \mu^+ \nu_\mu$ decays, the energy deposited in the EMC by muon is required to be less than 300 MeV and the maximum energy ($E_{\text{extra}\gamma}^{\text{max}}$) of the extra photons, which are not used in the DT event selection, is required to be less than 200 MeV.

The undetected neutrino in the SL decay is inferred by a kinematic variable $U_{\text{miss}} \equiv E_{\text{miss}} - |\vec{p}_{\text{miss}}|$, where $E_{\text{miss}} \equiv \sqrt{s} - \sum_j E_j$ is the missing energy and $\vec{p}_{\text{miss}} \equiv -\sum_j \vec{p}_j$ is the missing momentum. Here, the index j runs over all the particles used in the DT event selection, E_j and \vec{p}_j are the energy and momentum of the j -th particle in the e^+e^- rest frame. The U_{miss} distribution of the SL decays candidates is expected to peak near zero. To further suppress backgrounds from the hadronic decays $D_s^+ \rightarrow \phi(\eta, \eta') \pi^+$ and $\phi(\eta, \eta') \pi^+ \pi^0$ for semi-muonic decays, we define a variable $\delta E = E_{\text{beam}} - (E_{\phi(\eta, \eta')} + E_{\mu^+ \text{ as } \pi^+} + E_{\nu_\mu \text{ as } \pi^0})$, where $E_{\phi(\eta, \eta')}$ is the energy of $\phi(\eta, \eta')$ candidate, $E_{\mu^+ \text{ as } \pi^+}$ is the energy of μ^+ candidate by assuming it is pion, and $E_{\nu_\mu \text{ as } \pi^0}$ is the energy of missing particle by assuming to be π^0 (calculated with \vec{p}_{miss}). The DT candidate events are required to have δE within $(-0.080, -0.010)$, $(-0.100, 0)$, $(-0.070, -0.015)$ and $(-0.060, -0.015)$ GeV for $D_s^+ \rightarrow \phi \mu^+ \nu_\mu$, $\eta \mu^+ \nu_\mu$, $\eta'_{\pi^+\pi^-} \mu^+ \nu_\mu$ and $\eta'_{\gamma\rho^0} \mu^+ \nu_\mu$, respectively. Figure 2 shows the U_{miss} distributions of the accepted candidate events for the SL decays in data. The U_{miss} signal

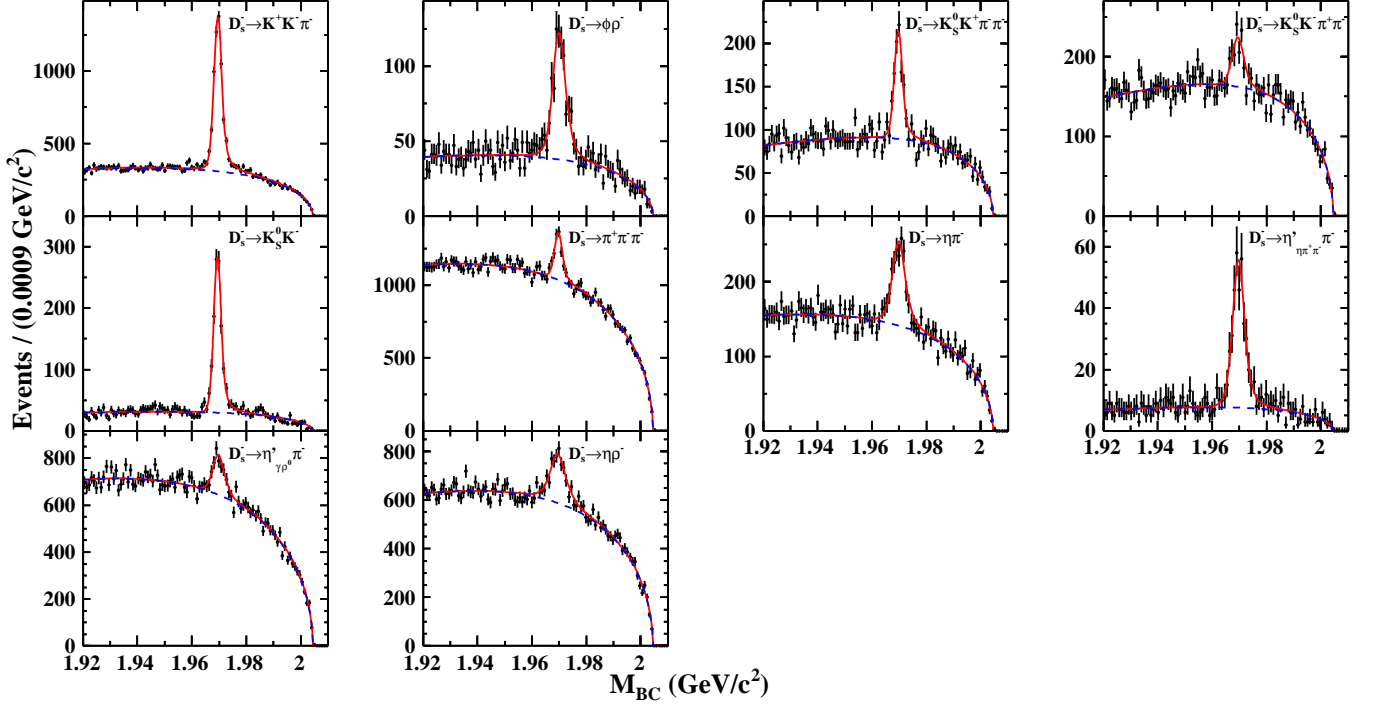


FIG. 1: (Color online) Fits to the M_{BC} distributions of the ST D_s^- decay modes. The dots with error bar are data, the red solid curves represent the total fits, and the blue dashed curves describe the fitted backgrounds.

TABLE I: Summary of the requirements on ΔE and M_{BC} , the ST yields in data (N_{ST}) and the ST efficiencies (ϵ_{ST}), which do not include the BFs for daughter particles π^0 , K_S^0 , ϕ , η and η' for the individual ST mode. The uncertainties are statistical only.

ST mode	ΔE (GeV)	M_{BC} (GeV/c ²)	N_{ST}^i	ϵ_{ST}^i (%)
$D_s^- \rightarrow K^+ K^- \pi^-$	(-0.020, 0.017)	(1.9635, 1.9772)	4820 ± 95	39.95 ± 0.09
$D_s^- \rightarrow \phi \rho^-$	(-0.036, 0.023)	(1.9603, 1.9820)	619 ± 39	10.88 ± 0.07
$D_s^- \rightarrow K_S^0 K^+ \pi^- \pi^-$	(-0.018, 0.014)	(1.9632, 1.9781)	581 ± 40	24.05 ± 0.17
$D_s^- \rightarrow K_S^0 K^- \pi^+ \pi^-$	(-0.016, 0.012)	(1.9621, 1.9777)	400 ± 50	22.51 ± 0.22
$D_s^- \rightarrow K_S^0 K^-$	(-0.019, 0.020)	(1.9640, 1.9761)	1065 ± 38	46.89 ± 0.21
$D_s^- \rightarrow \pi^+ \pi^- \pi^-$	(-0.026, 0.022)	(1.9624, 1.9787)	1500 ± 125	54.35 ± 0.19
$D_s^- \rightarrow \eta \pi^-$	(-0.052, 0.058)	(1.9599, 1.9823)	834 ± 56	48.36 ± 0.27
$D_s^- \rightarrow \eta' \pi^+ \pi^- \pi^-$	(-0.025, 0.024)	(1.9602, 1.9814)	325 ± 22	23.47 ± 0.22
$D_s^- \rightarrow \eta' \rho^0 \pi^-$	(-0.041, 0.033)	(1.9611, 1.9803)	1110 ± 106	37.11 ± 0.18
$D_s^- \rightarrow \eta \rho^-$	(-0.058, 0.041)	(1.9576, 1.9844)	1838 ± 120	26.11 ± 0.10
Total			13092 ± 247	

region is defined as $(-0.10, 0.10)$ GeV, in which we observe 28.0 ± 5.3 , 34.0 ± 5.8 , 64.0 ± 8.0 and 28.0 ± 5.3 candidate events for $D_s^+ \rightarrow \phi e^+ \nu_e$, $\phi \mu^+ \nu_\mu$, $\eta \mu^+ \nu_\mu$, and $\eta' \pi^+ \pi^-$ and $\gamma \rho^0 \mu^+ \nu_\mu$, respectively.

Some background events may also survive the selection criteria of the SL decays of interest. The backgrounds can be classed into two categories. Those background events, in which the ST D_s^- meson is reconstructed correctly but the SL decay is mis-identified, are defined as ‘real- D_s^- ’ background. The other background events, in which the ST D_s^- meson is reconstructed incorrectly, are called as ‘non- D_s^- ’ background. The number of ‘real- D_s^- ’ background events is estimated by analyzing the inclusive MC sample. While the

‘non- D_s^- ’ background yield is evaluated by using the events of data within the M_{BC} sideband region, which is defined to be $(1.920, 1.950)$ and $(1.990, 2.000)$ GeV/c² on the M_{BC} distribution. The background yield in the M_{BC} sideband region is then scaled by the ratio of the background integral areas between the M_{BC} signal and sideband regions.

The DT yields observed in data (N_{DT}^{obs}), the expected number of ‘real- D_s^- ’ and ‘non- D_s^- ’ background ($N_{\text{real-}D_s^-}^{\text{bkg}}$ and $N_{\text{non-}D_s^-}^{\text{bkg}}$) as well as the weighted efficiencies of detecting the SL decays according to the ST yields of data ($\bar{\epsilon}_{SL}$) are summarized in Table II, where the efficiencies $\bar{\epsilon}_{SL}$ do not include the BFs of ϕ , η and η' in the SL decays. So, the BFs for

TABLE II: The numbers used to extract the BF of SL decay as well as the resultant BF. The uncertainties are statistical only.

Decay mode	$N_{\text{DT}}^{\text{obs}}$	$N_{\text{real}-D_s^-}^{\text{bkg}}$	$N_{\text{non}-D_s^-}^{\text{bkg}}$	$\bar{\epsilon}_{\text{SL}} (\%)$	$\mathcal{B}_{\text{SL}} (\%)$
$D_s^+ \rightarrow \phi e^+ \nu_e$	28.0 ± 5.3	1.6 ± 0.2	$0.0^{+0.1}_{-0.0}$	18.2 ± 0.1	2.26 ± 0.45
$D_s^+ \rightarrow \phi \mu^+ \nu_\mu$	34.0 ± 5.8	6.8 ± 0.5	5.1 ± 1.6	17.8 ± 0.1	1.94 ± 0.53
$D_s^+ \rightarrow \eta \mu^+ \nu_\mu$	64.0 ± 8.0	7.0 ± 0.5	12.6 ± 2.6	35.6 ± 0.2	2.42 ± 0.46
$D_s^+ \rightarrow \eta' \mu^+ \nu_\mu$	28.0 ± 5.3	3.7 ± 0.4	14.0 ± 2.6	16.2 ± 0.1	1.06 ± 0.54

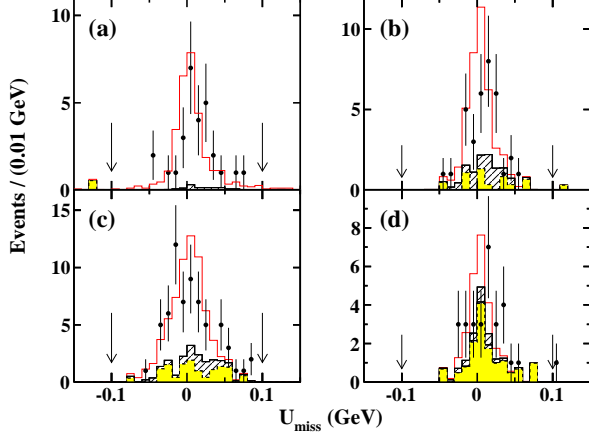


FIG. 2: Distributions of U_{miss} of the candidate events for $D_s^+ \rightarrow$ (a) $\phi e^+ \nu_e$, (b) $\phi \mu^+ \nu_\mu$, (c) $\eta \mu^+ \nu_\mu$ and (d) $\eta' \mu^+ \nu_\mu$ where the pair of arrows represent the signal region. The dots with error bar are data, the red histograms are inclusive MC, and the yellow and oblique-line hatched histograms represent the scaled ‘real- D_s^- ’ and ‘non- D_s^- ’ backgrounds.

the SL decays are determined by

$$\mathcal{B}_{\text{SL}} = \frac{N_{\text{DT}}^{\text{obs}} - N_{\text{real}-D_s^-}^{\text{bkg}} - N_{\text{non}-D_s^-}^{\text{bkg}}}{N_{\text{ST}}^{\text{tot}} \bar{\epsilon}_{\text{SL}} \mathcal{B}_{\text{sub}}}, \quad (4)$$

where \mathcal{B}_{sub} denotes the BF for the daughter particles ϕ , η and η' quoted from PDG [4]. Inserting the numbers of $N_{\text{DT}}^{\text{obs}}$, $N_{\text{real}-D_s^-}^{\text{bkg}}$, $N_{\text{non}-D_s^-}^{\text{bkg}}$, $N_{\text{ST}}^{\text{tot}}$, $\bar{\epsilon}_{\text{SL}}$ and \mathcal{B}_{sub} in Eq. (4), we obtain the BF for $D_s^+ \rightarrow \phi e^+ \nu_e$, $\phi \mu^+ \nu_\mu$, $\eta \mu^+ \nu_\mu$ and $\eta' \mu^+ \nu_\mu$, respectively. These results are summarized in Table II.

IV. SYSTEMATIC UNCERTAINTIES

In the BF measurements using DT method, the systematic uncertainties arising from the ST selection are almost canceled. Main systematic uncertainties in the measurements for BF of SL decays are discussed below.

a. *ST yield.* The uncertainty of the total ST yield is estimated to be 1.8% by comparing the integrated and counted ST yields (calculated by subtracting the background yields from total events without performing a fit) in the M_{BC} signal region.

b. *Tracking and PID.* The uncertainties in the tracking and PID for charged kaon and pion are investigated with the control sample of DT hadronic $D\bar{D}$ events and are assigned to be 1.0% and 1.0% per track individually. The efficiencies of the tracking and PID for electron and muon are studied by varying with the polar angle $\cos \theta$ and momentum with the control samples $e^+e^- \rightarrow \gamma e^+e^-$ and $e^+e^- \rightarrow \gamma \mu^+\mu^-$ events, respectively. These efficiencies are weighted according to $\cos \theta$ and momentum distributions of the electron and muon in the SL decays. The resultant differences of the two-dimensional weighted tracking and PID efficiencies for electron and muon between data and MC simulation are regarded as the relevant uncertainties.

c. *$E_{\text{extra}\gamma}^{\text{max}}$ requirement.* The efficiency of $E_{\text{extra}\gamma}^{\text{max}}$ requirement is investigated with fully reconstructed DT hadronic decays $\psi(4040) \rightarrow D^*\bar{D} + c.c..$ The difference of the efficiencies with the requirement of $E_{\text{extra}\gamma}^{\text{max}} < 200$ MeV between data and MC simulation is found to be $(1.9 \pm 0.6)\%$. To be conservative, we assign 2.5% to be the associated systematic uncertainty.

d. *ϕ (η , η') reconstruction.* The reconstruction efficiencies for the ϕ , η and η' candidates, which include the mass window requirement and photon selection, are estimated with the control samples of $D^+ \rightarrow \phi \pi^+$, $D^0 \rightarrow K_S^0 \eta$, $D^0 \rightarrow K_S^0 \eta'_{\pi^+\pi^-\eta}$ and $K_S^0 \eta'_{\gamma\rho^0}$, respectively. The differences of efficiencies between data and MC simulation are estimated to be 0.4%, 2.3%, 2.5% and 2.8% for ϕ , η , $\eta'_{\pi^+\pi^-\eta}$ and $\eta'_{\gamma\rho^0}$, respectively, which are assigned as the associated uncertainties.

e. *δE requirement.* The uncertainties from δE requirements are estimated by varying the δE requirements by $\pm 10\%$. The changes of the BF, which are 0.7%, 1.2%, 1.7% and 1.8% for $D_s^+ \rightarrow \phi \mu^+ \nu_\mu$, $\eta \mu^+ \nu_\mu$, $\eta'_{\pi^+\pi^-\mu^+ \nu_\mu}$ and $\eta'_{\gamma\rho^0} \mu^+ \nu_\mu$, respectively, are taken as the corresponding uncertainties.

f. *Background subtraction.* Two aspects uncertainties associated with background subtraction are considered separately. The ‘real- D_s^- ’ background is estimated with the inclusive MC samples, thus, we vary the quoted BF of the main background sources $D_s^+ \rightarrow \phi \mu^+ \nu_\mu$, $\phi \rho^+$, $\eta \rho^+$, $\eta'_{\pi^+\pi^-\rho^+}$ and $\eta'_{\gamma\rho^0} \rho^+$ by 1σ quoted in PDG [4]. The ‘non- D_s^- ’ background is estimated with the candidate events in the M_{BC} sideband region. We then shift

TABLE III: Systematic uncertainties (in %) in the BF measurements. The sources tagged with ‘c’ are regarded as common systematic uncertainties between the two η' decay modes.

Source	$D_s^+ \rightarrow \phi e^+ \nu_e$	$D_s^+ \rightarrow \phi \mu^+ \nu_\mu$	$D_s^+ \rightarrow \eta \mu^+ \nu_\mu$	$D_s^+ \rightarrow \eta'_{\pi^+\pi^-} \mu^+ \nu_\mu$	$D_s^+ \rightarrow \eta'_{\rho^0} \mu^+ \nu_\mu$
ST yield	1.8	1.8	1.8	1.8 ^c	1.8 ^c
Tracking for K^+ (π^+)	2.0	2.0	—	2.0 ^c	2.0 ^c
PID for K^+ (π^+)	2.0	2.0	—	2.0 ^c	2.0 ^c
Tracking for e^+ (μ^+)	1.0	1.0	1.0	1.0 ^c	1.0 ^c
PID for e^+ (μ^+)	0.9	2.4	1.5	1.9 ^c	1.9 ^c
$E_{\text{extra}\gamma}^{\text{max}}$ requirement	—	—	2.5	2.5 ^c	2.5 ^c
$\phi(\eta, \eta')$ reconstruction	0.4	0.4	2.3	2.5	2.8
δE requirement	—	0.7	1.2	1.7	1.8
Background subtraction	0.2	1.5	1.2	3.1	3.0
MC statistics	0.5	0.6	0.4	0.6	0.6
MC model	1.4	1.1	0.7	2.5	2.2
BFs of ϕ and η'	1.0	1.0	0.5	1.6	1.7
Total	4.0	4.8	4.7	7.0	7.1

the M_{BC} sideband region by $\pm 5 \text{ MeV}/c^2$. The quadratic sum of these two effects on the measured BFs, which are 0.2%, 1.5%, 1.2%, 3.1% and 3.0% for $D_s^+ \rightarrow \phi e^+ \nu_e$, $\phi \mu^+ \nu_\mu$, $\eta \mu^+ \nu_\mu$, $\eta'_{\pi^+\pi^-} \mu^+ \nu_\mu$ and $\eta'_{\rho^0} \mu^+ \nu_\mu$, respectively, are treated as the systematic uncertainties.

- g. *MC statistics.* The uncertainties in the weighted efficiencies are mainly due to limited MC statistics, which are 0.5%, 0.6%, 0.4%, 0.6% and 0.6% for $D_s^+ \rightarrow \phi e^+ \nu_e$, $\phi \mu^+ \nu_\mu$, $\eta \mu^+ \nu_\mu$, $\eta'_{\pi^+\pi^-} \mu^+ \nu_\mu$ and $\eta'_{\rho^0} \mu^+ \nu_\mu$, respectively. The effects of the statistical uncertainty of ST yields of data is negligible for the weighting efficiencies.
- h. *MC model.* The uncertainty associated with MC model is studied with an alternative SL form-factor model, *i.e.*, the simple pole model [22]. The resultant differences on DT efficiencies with respect to the nominal values, which are 1.4%, 1.1%, 0.7%, 2.5% and 2.2% for $D_s^+ \rightarrow \phi e^+ \nu_e$, $\phi \mu^+ \nu_\mu$, $\eta \mu^+ \nu_\mu$, $\eta'_{\pi^+\pi^-} \mu^+ \nu_\mu$ and $\eta'_{\rho^0} \mu^+ \nu_\mu$, respectively, are considered as the associated systematic uncertainties.
- i. *BFs of ϕ and η' .* The BFs for $\phi \rightarrow K^+ K^-$, $\eta \rightarrow \gamma\gamma$, $\eta' \rightarrow \eta\pi^+\pi^-$ and $\eta' \rightarrow \gamma\rho^0$ are quoted from the PDG [4]. Their uncertainties are 1.0%, 0.5%, 1.6% and 1.7%, respectively.

The individual systematic uncertainties discussed above are summarized in Table III and the total systematic uncertainties are the quadratic sum of the individual ones. The sources tagged with ‘c’ are common systematic uncertainties between the two η' decay modes and the other sources are independent. Finally, we assign 7.1% as the total systematic uncertainty for $D_s^+ \rightarrow \eta' \mu^+ \nu_\mu$.

V. SUMMARY

In summary, by analyzing the 482 pb^{-1} data collected at $\sqrt{s} = 4.009 \text{ GeV}$ with the BESIII detector, we determine the BFs for the SL decays $D_s^+ \rightarrow \phi e^+ \nu_e$, $\phi \mu^+ \nu_\mu$, $\eta \mu^+ \nu_\mu$ and $\eta' \mu^+ \nu_\mu$. Table IV presents the comparisons of the measured BFs with the world average values. The BFs of the semi-muonic decays $D_s^+ \rightarrow \phi \mu^+ \nu_\mu$, $\eta \mu^+ \nu_\mu$ and $\eta' \mu^+ \nu_\mu$ are determined for the first time and are compatible with those of the corresponding semi-electronic decays [4]. The BF of $D_s^+ \rightarrow \phi e^+ \nu_e$ agrees with the world average value [4] within uncertainties. And, the results are consistent with previous experimental measurements and support that the ratio of D_s^+ and $D^{0(+)}$ differs from unity, there is an indication of difference between $D^{0(+)}$ and D_s^+ meson SL decay widths [2]. Combining the previous BESIII measurements for semi-electronic decays [8] and this work, we calculate the ratios between the semi-electronic and semi-muonic decays, to be $\mathcal{B}(D_s^+ \rightarrow \phi \mu^+ \nu_\mu)/\mathcal{B}(D_s^+ \rightarrow \phi e^+ \nu_e) = 0.86 \pm 0.29$, $\mathcal{B}(D_s^+ \rightarrow \eta \mu^+ \nu_\mu)/\mathcal{B}(D_s^+ \rightarrow \eta e^+ \nu_e) = 1.05 \pm 0.24$ and $\mathcal{B}(D_s^+ \rightarrow \eta \mu^+ \nu_\mu)/\mathcal{B}(D_s^+ \rightarrow \eta e^+ \nu_e) = 1.14 \pm 0.68$ individually, where most of systematic uncertainties are canceled. The ratios are consistent with 1 within the uncertainties, and no obvious lepton universality violation is observed. Moreover, the ratio of $\mathcal{B}(D_s^+ \rightarrow \eta \mu^+ \nu_\mu)$ over $\mathcal{B}(D_s^+ \rightarrow \eta' \mu^+ \nu_\mu)$ is calculated to be 0.44 ± 0.23 , which is in agreement with those of previous measurements [5, 7, 8, 23] within uncertainties and provides complementary data to probe the $\eta - \eta'$ -glueball mixing.

VI. ACKNOWLEDGMENTS

The BESIII collaboration thanks the staff of BEPCII and the IHEP computing center for their strong support. This

TABLE IV: Summary of the BF's and comparing with the world average values [4].

μ^+ mode	$\mathcal{B}_{\text{BESIII}} (\%)$	$\mathcal{B}_{\text{PDG}} (\%)$	e^+ mode	$\mathcal{B}_{\text{BESIII}} (\%)$	$\mathcal{B}_{\text{PDG}} (\%)$
$D_s^+ \rightarrow \phi \mu^+ \nu_\mu$	$1.94 \pm 0.53 \pm 0.09$	–	$D_s^+ \rightarrow \phi e^+ \nu_e$	$2.26 \pm 0.45 \pm 0.09$	2.39 ± 0.23
$D_s^+ \rightarrow \eta \mu^+ \nu_\mu$	$2.42 \pm 0.46 \pm 0.11$	–	$D_s^+ \rightarrow \eta e^+ \nu_e$	$2.30 \pm 0.31 \pm 0.08$ [8]	2.28 ± 0.24
$D_s^+ \rightarrow \eta' \mu^+ \nu_\mu$	$1.06 \pm 0.54 \pm 0.07$	–	$D_s^+ \rightarrow \eta' e^+ \nu_e$	$0.93 \pm 0.30 \pm 0.05$ [8]	0.68 ± 0.16

work is supported in part by National Key Basic Research Program of China under Contract No. 2015CB856700; National Natural Science Foundation of China (NSFC) under Contracts Nos. 11235011, 11335008, 11425524, 11625523, 11635010, 11675200; the Chinese Academy of Sciences (CAS) Large-Scale Scientific Facility Program; the CAS Center for Excellence in Particle Physics (CCEPP); Joint Large-Scale Scientific Facility Funds of the NSFC and CAS under Contracts Nos. U1332201, U1532257, U1532258; CAS under Contracts Nos. KJCX2-YW-N29, KJCX2-YW-N45, QYZDJ-SSW-SLH003; 100 Talents Program of CAS; National 1000 Talents Program of China; INPAC and Shanghai Key Laboratory for Particle Physics and Cosmology; German Research Foundation DFG under Contracts Nos. Collaborative Research Center CRC

1044, FOR 2359; Istituto Nazionale di Fisica Nucleare, Italy; Joint Large-Scale Scientific Facility Funds of the NSFC and CAS; Koninklijke Nederlandse Akademie van Wetenschappen (KNAW) under Contract No. 530-4CDP03; Ministry of Development of Turkey under Contract No. DPT2006K-120470; National Natural Science Foundation of China (NSFC) under Contract No. 11505010; National Science and Technology fund; The Swedish Research Council; U. S. Department of Energy under Contracts Nos. DE-FG02-05ER41374, DE-SC-0010118, DE-SC-0010504, DE-SC-0012069; University of Groningen (RuG) and the Helmholtzzentrum fuer Schwerionenforschung GmbH (GSI), Darmstadt; WCU Program of National Research Foundation of Korea under Contract No. R32-2008-000-10155-0

-
- [1] M. B. Voloshin, Phys. Lett. B **515**, 74 (2001).
[2] D. M. Asner *et al.* (CLEO Collaboration), Phys. Rev. D **81**, 052007 (2010).
[3] D. Scora and N. Isgur, Phys. Rev. D **52**, 2783 (1995).
[4] C. Patrignani *et al.* (Particle Data Group), Chin. Phys. C, **40**, 100001 (2016).
[5] J. Yelton *et al.* (CLEO Collaboration), Phys. Rev. D **80**, 052007 (2009).
[6] B. Aubert *et al.* (BaBar Collaboration), Phys. Rev. D **78**, 051101 (2008).
[7] J. Hietala, D. Cronin-Hennessy, T. Pedlar and I. Shipsey, Phys. Rev. D **92**, 012009 (2015).
[8] M. Ablikim *et al.* (BESIII Collaboration), Phys. Rev. D **94**, 112003 (2016).
[9] C. D. Donato, G. Ricciardi and I. Bigi, Phys. Rev. D **85**, 013016 (2012).
[10] V. V. Anisovich, D. V. Bugg, D. I. Melikhov, V. A. Nikonov, Phys. Lett. B **404**, 166 (1997).
[11] M. Ablikim *et al.* (BESIII Collaboration), Chin. Phys. C **39**, 093001 (2015).
[12] M. Ablikim *et al.* (BESIII Collaboration), Nucl. Instrum. Meth. A **614**, 345 (2010).
[13] S. Agostinelli *et al.* (GEANT4 Collaboration), Nucl. Instrum. Meth. A **506**, 250 (2003).
[14] S. Jadach, B. F. L. Ward and Z. Was, Comput. Phys. Commun. **130**, 260 (2000); S. Jadach, B. F. L. Ward and Z. Was, Phys. Rev. D **63**, 113009 (2001).
[15] D. J. Lange, Nucl. Instrum. Meth. A **462**, 152 (2001).
[16] R. G. Ping *et al.*, Chin. Phys. C **32**, 599 (2008).
[17] E. A. Kurav and V. S. Fadin, Sov. J. Nucl. Phys. **41**, 466 (1985).
[18] E. Barberio and Z. Was, Comput. Phys. Commun. **79**, 291 (1994).
[19] D. Cronin-Hennessy *et al.* (CLEO Collaboration), Phys. Rev. D **80**, 072001 (2009).
[20] J. C. Chen, G. S. Huang, X. R. Qi *et al.*, Phys. Rev. D **62**, 034003 (2000).
[21] H. Albrecht *et al.* (ARGUS Collaboration), Phys. Lett. B **241**, 278 (1990).
[22] D. Becirevic and A. B. Kaidalov, Phys. Lett. B **478**, 417 (2000).
[23] G. Brandenburg *et al.* (CLEO Collaboration), Phys. Rev. Lett. **75**, 3804 (1995).